Sheddable Ternary Nanoparticles for Tumor Acidity-Targeted siRNA Delivery

Xian-Zhu Yang,[†,‡] Jin-Zhi Du,[§] Shuang Dou,[†] Cheng-Qiong Mao,[†] Hong-Yan Long,[§] and Jun Wang[†,*]

[†]CAS Key Laboratory of Brain Function and Disease, and School of Life Sciences, University of Science and Technology of China, Hefei, Anhui 230027, People's Republic of China, [‡]Hefei National Laboratory for Physical Sciences at the Microscale, University of Science and Technology of China, Hefei, Anhui 230027, People's Republic of China, and [§]Department of Polymer Science and Engineering, University of Science and Technology of China, Hefei, Anhui 230026, People's Republic of China

ABSTRACT

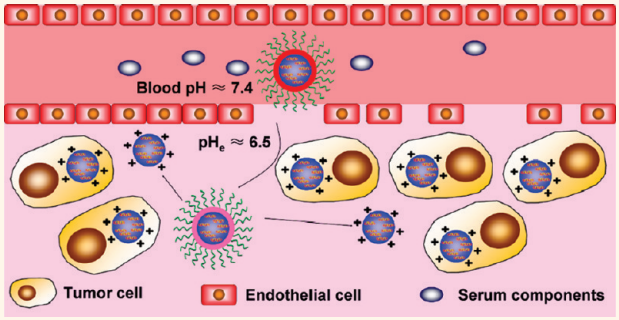

Drug delivery systems for cancer therapy usually need to be sterically stabilized by a poly(ethylene glycol) (PEG) layer during blood circulation to minimize nonspecific interactions with serum components. However, PEGylation significantly reduces cellular uptake of the delivery systems after they accumulate at the tumor site, which markedly impairs the *in vivo* antitumor efficiency. Here, we develop a ternary small interfering RNA (siRNA) delivery system with tumor acidity-activated sheddable PEG layer to overcome the challenge. The sheddable nanoparticle is fabricated by introducing a tumor acidity-responsive PEGylated anionic polymer to the surface of positively charged polycation/siRNA complexes *via* electrostatic interaction. We show clear evidence that introducing the PEGylated anionic polymer to the surface of a nanoparticle markedly reduces its nonspecific interactions with protein. We further demonstrate that the nanoparticle is capable of deshielding the PEG layer at the slightly acidic tumor extracellular microenvironment to facilitate the delivery of siRNA to the tumor cells after accumulation at the tumor site. Accordingly, this promotes the RNA-interfering efficiencies and enhances the inhibition of tumor growth. Such delivery system with the ability to deshield the PEG layer at the target tissues has remarkable potential in cancer therapy.

KEYWORDS: sheddable nanoparticles · pH-responsive · tumor acidity · siRNA delivery · nanotechnology

Small interfering RNA (siRNA) has rapidly emerged as a promising candidate for the treatment of numerous diseases,[1−4] but its therapeutic efficacy is hampered by difficulties in its systemic *in vivo* delivery to targeted tissues and cells.[5] To overcome the obstacles, a few vehicles have been developed to deliver siRNA.[6] They have shown promising efficacy in specific gene silencing and the treatment of various diseases. The delivery systems can be mainly divided into two categories: positively charged nanoparticles with or without PEGylation. Positively charged nanoparticles without PEGylation can efficiently down-regulate gene expression *in vitro*.[7,8] However, these nanoparticles usually fail to achieve satisfactory efficacy for systemic siRNA delivery.[9] One key reason is due to the nonspecific interaction between positively charged polyplex particles and serum components, leading to their severe aggregation and rapid clearance from the circulation by the reticuloendothelial system following systemic administration.[10−12] PEGylation sterically stabilizes nanoparticles, which minimizes the nonspecific interaction *in vivo*,[13,14] and thus prolongs the circulation time, facilitating tumoral accumulation *via* enhanced permeation and retention (EPR) effects.[15,16] Unfortunately, PEGylation markedly reduces their cellular uptake in tumor tissues,[17−20] significantly limiting the gene silencing and antitumor efficiency of siRNA *in vivo*. The ideal delivery systems of siRNA should be capable of simultaneously extending circulation time in blood to enhance tumor accumulation but becoming active at the tumor site to promote cellular uptake.

The extracellular pH (pH$_e$) of tumor tissue (*ca.* pH 6.5) is significantly lower than that of normal tissue and blood (*ca.* pH 7.4) due to the hypoxia-induced production of excess lactate and protons in tumor extracellular microenvironments.[21−23] The acidic environment of tumors has been utilized to trigger the disassembly of delivery systems with subsequent drug release or to re-expose cells targeting ligands that are shielded during circulation.[24−27] Recently, Poon *et al.* have reported important results that fluorescent nanoparticles with the ability to remove the PEG stealth layer at

* Address correspondence to jwang699@ustc.edu.cn.

Received for review November 2, 2011 and accepted December 3, 2011.

Published online December 03, 2011
10.1021/nn204240b

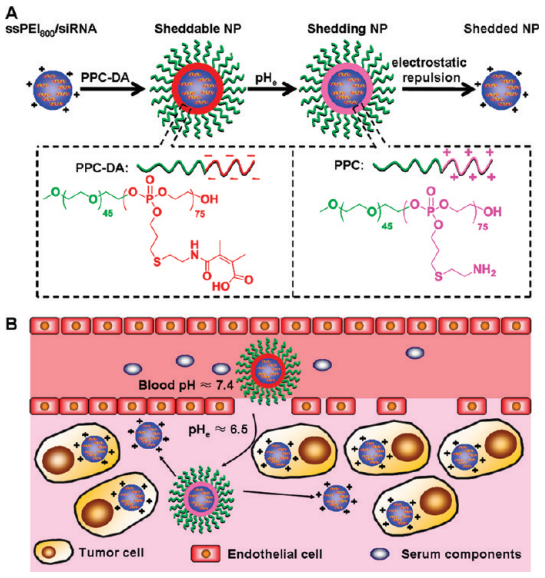

Scheme 1. (A) Shielding and deshielding of the positively charged ssPEI$_{800}$/siRNA nanoparticles by the PEG shell in the acidic environment of the tumor. The ssPEI$_{800}$/siRNA nanoparticles are coated with the PEGylated anionic polymer PPC-DA to form the sheddable nanoparticles (NP). At the extracellular pH (pH$_e$) of tumor tissue, the sheddable NPs deshield the degraded PEGylated polymer layer (PPC) and re-expose the ssPEI$_{800}$/siRNA nanoparticles (shedded NP). (B) Schematic illustration of the stealth property and promoted tumoral cell uptake of sheddable nanoparticles. The sheddable NPs minimize nonspecific interactions with serum components and deshield the PEG layer at the tumor site to re-expose the positive charges, leading to promoted cell internalization.

pH values less than pH 8.0 and re-expose the positively charged surface improve tumor cell uptake following intravenous injection.[28] The results suggest nanoparticles with the charge conversional ability by deshielding the PEG layer at tumor acidity may exhibit superior efficacy in delivering therapeutic agents *in vivo*. Sethuraman *et al.* have demonstrated the enhanced transfection efficiency of a tumor acidity-responsive sulfonamide/poly(ethylenimine)/pDNA delivery *in vitro*,[29] but the *in vivo* efficacy has not been verified. Herein, we report a ternary sheddable nanoparticular system (S-NP) for tumor acidity-targeted siRNA delivery by introducing a tumor acidity-responsive PEGylated anionic polymer (mPEG$_{45}$-*b*-PAEP$_{75}$-Cya-DMMA, PPC-DA, where the subscript number represents degree of polymerization of each block) layer to the surface of positively charged ssPEI$_{800}$/siRNA nanoparticles through electrostatic interaction (Scheme 1A). The amide bonds of PPC-DA are stable at a neutral pH but promptly degrade under the slightly acidic environmental conditions of tumors to expose positively charged amino groups.[30] The ssPEI$_{800}$/siRNA nanoparticles are shielded by such a PEGylated polymer, which markedly minimizes nonspecific interactions with serum components during circulation and significantly improves their accumulation in the tumor site (Scheme 1B). However, the exposure of amino groups of the PEGylated polymer, triggered by tumor acidity, leads to its electrostatic repulsion to the highly and positively charged ssPEI$_{800}$/siRNA nanoparticles, deshielding the PEGylated polymer layer from the sheddable nanoparticles. Accordingly, this promotes its uptake by the tumor cell and further enhances the RNA-interfering and tumor growth suppression efficiencies.

RESULTS AND DISCUSSION

Preparation and Characterization of S-NP. The ternary S-NP for tumor acidity-targeted siRNA delivery was prepared by introducing a tumor acidity-responsive PEGylated anionic polymer PPC-DA to the surface of positively charged ssPEI$_{800}$/siRNA nanoparticles through electrostatic interaction. In order to obtain the tumor acidity-responsive PPC-DA, we first synthesized the diblock polymer mPEG$_{45}$-*b*-PAEP$_{75}$. The average degree of polymerization of PAEP was 75, which was calculated based on its ^{1}H NMR analysis. The mPEG$_{45}$-*b*-PAEP$_{75}$-Cya (PPC) was then synthesized *via* the thiol−ene "click" reaction of mPEG$_{45}$-*b*-PAEP$_{75}$ with cysteamine (Cya), and the extent of Cya conjugation was about 100% according to the ^{1}H NMR analysis.[30] The PPC was further reacted with 2,3-dimethylmaleic anhydride (DMMA) to obtained the tumor acidity-responsive PPC-DA. As a control, mPEG$_{45}$-*b*-PAEP$_{75}$-Cya-SA (PPC-SA), stable under the acidity of the tumor, was synthesized by reacting PPC with succinic anhydride (SA). The extent of DMMA or SA conjugation to PPC was approximately 75% according to the ^{1}H NMR analyses. Details of the synthesis and characterization procedures are given in the Supporting Information.

The bioreducible polymer ssPEI$_{800}$ was obtained by the linking reaction of dithiobis(succinimidyl propionate) with branched polyethylenimine (M_w = 800), which showed high transfection efficiency with significantly low cytotoxicity.[31] ssPEI$_{800}$ can efficiently bind siRNA to form ssPEI$_{800}$/siRNA nanoparticles at a molar ratio of nitrogen in the ssPEI$_{800}$ to phosphate in siRNA (N/P ratio) of above 4:1, as shown by the agarose retardation assay (Figure S1 in Supporting Information). The PPC-DA was added to the positively charged ssPEI$_{800}$/siRNA nanoparticles to form S-NP, which contained a ternary structure of PPC-DA/ssPEI$_{800}$/siRNA. Although it was possible that ssPEI$_{800}$/siRNA nanoparticles could form between ssPEI$_{800}$ and PPC-DA, gel electrophoresis analyses showed that the introduction of the anionic PPC-DA polymer did not interfere with the formation of S-NP. No significant release of siRNA from the ssPEI$_{800}$/siRNA nanoparticles was observed with the addition of different amounts of PPC-DA (Figure S2).

The ssPEI$_{800}$/siRNA nanoparticles and ternary S-NP observed by the transmission electronic microscopic image both showed compact and spherical morphology (Figure 1A,B). On the other hand, the average size of the ssPEI$_{800}$/siRNA nanoparticles was 79.6 ± 12.7 nm

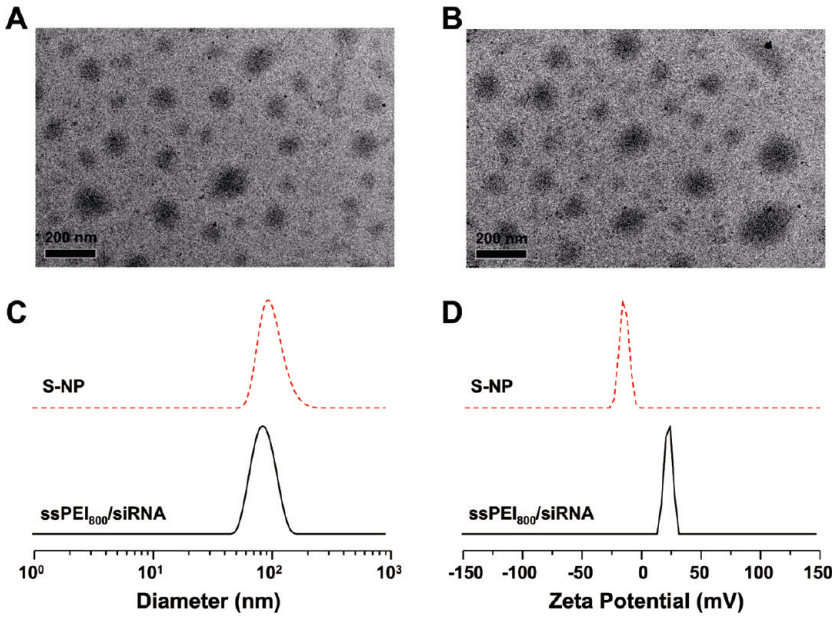

Figure 1. (A,B) Transmission electronic microscopic image of the ssPEI$_{800}$/siRNA nanoparticles (A) and ternary S-NP (B) (scale bar: 200 nm). (C,D) Intensity distribution of particle size (C) and zeta-potential (D) of S-NP and the ssPEI$_{800}$/siRNA nanoparticles.

(PDI = 0.164), which slightly increased to 91.0 ± 16.4 nm (PDI = 0.194) after the coating of PPC-DA. As expected, however, the zeta-potential of S-NP was negative (−14.7 mV) from the positively charged surface (24.0 mV) of the ssPEI$_{800}$/siRNA nanoparticles due to the electrostatic assembly of PPC-DA on the ssPEI$_{800}$/siRNA nanoparticles (Figure 1C,D). The unsheddable control nanoparticles PPC-SA/ssPEI$_{800}$/siRNA (unS-NP) showed similar size and zeta-potential transitions (data not shown).

PEG Shielding of Positively Charged Nanoparticles Reduces Nonspecific Interactions with Protein. PEGylation and the negatively charged surfaces of nanoparticles minimize its nonspecific interactions with serum components, thus potentially extending the blood circulation of nanoparticles and improving accumulation in the tumor following systemic *in vivo* administration.[13,32] In order to demonstrate this, we incubated the ssPEI$_{800}$/siRNA nanoparticles, unS-NP, or S-NP with bovine serum albumin (BSA, 0.25 mg/mL) in phosphate buffered saline (PBS, pH 7.4, 0.01 M) and determined the size of the nanoparticles at various incubation times. The particle sizes of unS-NP and S-NP were only slightly increased with incubation, unlike the size of the ssPEI$_{800}$/siRNA nanoparticles, which exhibited significantly large particles and severe aggregation in the short term (Figure 2). This phenomenon showed that the stability of the ssPEI$_{800}$/siRNA nanoparticles with serum protein can be enhanced by introducing a PEG layer to the surface.

S-NPs Detach the PEG Layer at Tumor Acidity. It has been demonstrated that DMMA-modified amines are stable under neutral pH conditions, but that the resulting amide bonds promptly degrade under slightly acidic

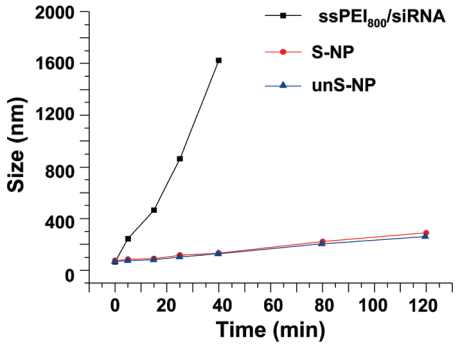

Figure 2. Changes in particle size of the ssPEI$_{800}$/siRNA nanoparticles, unS-NP, and S-NP following incubation with bovine serum albumin (0.25 mg mL^{-1}) at pH 7.4.

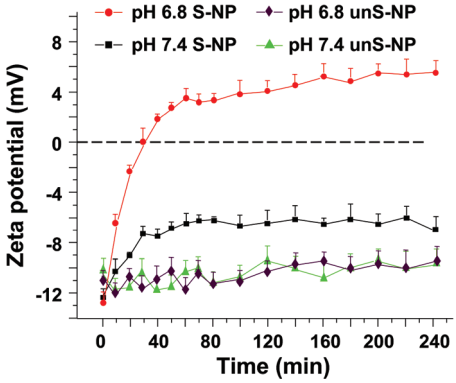

Figure 3. Zeta-potential changes in S-NP and unS-NP as a function of incubation time at pH 6.8 and 7.4.

environmental conditions in tumors.[33,34] To further demonstrate the fact that S-NPs can deshield the PEG shell at pH$_e$, we monitored changes in the zeta-potential of nanoparticles after incubation with PBS at pH 6.8

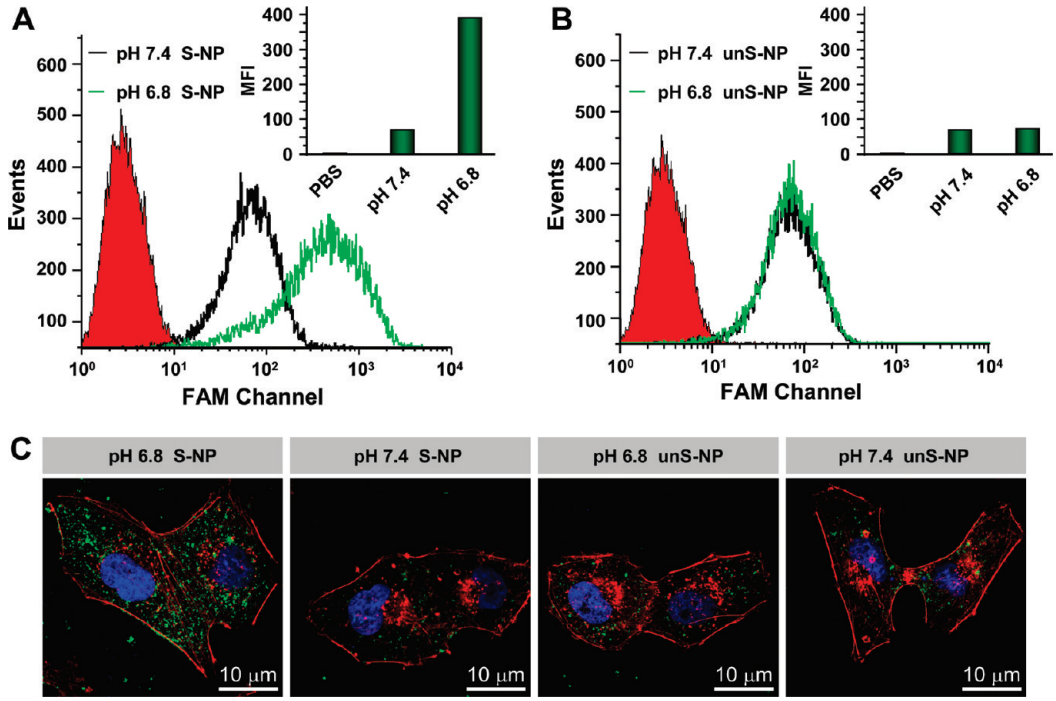

Figure 4. (A,B) Flow cytometric analyses of MDA-MB-231 cells after 2 h incubation with FAM-siRNA loaded S-NP (A) or unS-NP (B) at pH 6.8 or 7.4. Quantification of cell internalization is shown by mean fluorescence intensity (MFI) in the inset. The dose of FAM-siRNA was 200 nM in the cell culture. (C) Internalization of S-NP or unS-NP by MDA-MB-231 cells observed by confocal laser scanning microscopy. Cells were cultured with nanoparticles carrying FAM-siRNA (green) at different pH for 2 h incubation. Cell cytoskeleton F-actin and cell nuclei were counterstained with Alexa Fluor 568 phalloidin (red) and DAPI (blue), respectively. The dose of FAM-siRNA was 200 nM.

and 37 °C. Figure 3 shows that the zeta-potential of S-NP significantly increased at pH 6.8, reaching 0 mV within 30 min and gradually becoming positive. On the contrary, the incubation of S-NP at pH 7.4 only led to a slight and slow increase in the zeta-potential, and S-NP retained the negative surface after 4 h of incubation. Nevertheless, unS-NP was not affected by the pH of PBS buffer, exhibiting an unchanged zeta-potential following incubation at either pH 7.4 or pH 6.8. These results demonstrated that the exposure of S-NP at pH 6.8 triggered the pH_e-activated degradation of amide bonds of PPC-DA, generating positively charged amino groups,[30] which further led to strong electrostatic repulsion to positively charged $ssPEI_{800}$/siRNA nanoparticles and the formation of shedded nanoparticles (Scheme 1A).

Deshielding the PEG Layer of S-NP Facilitates Cell Internalization. Previous studies showed that negatively charged PEGylated nanoparticles inhibited cellular uptake in a remarkable manner.[18,28,35] Deshielding the PEG layer from S-NP and re-exposing the positively charged surface at pH_e could thus enhance the cellular uptake of nanoparticles. This hypothesis was verified by determining the cellular internalization of S-NP in MDA-MB-231 cells. The cells were cultured with fluorescent FAM-siRNA-loaded S-NP at pH 7.4 or 6.8. As shown in Figure 4A, after 2 h of incubation with S-NP at pH 6.8, a much stronger cellular fluorescence was detected compared to cells cultured with S-NP at pH 7.4. In contrast, the internalization of unS-NP by MDA-MB-231 cells was not significantly affected by pH, where very similar mean fluorescence intensities to the cells treated with S-NP at pH 7.4 (Figure 4B) were shown.

The cellular uptake was further corroborated by confocal laser scanning microscopic observations. The cells were cultured with S-NP or unS-NP carrying FAM-siRNA at pH 7.4 or 6.8. After 2 h of incubation, the cytoskeleton F-actin and the cell nuclei were counterstained with Alexa Fluor 568 phalloidin and 6-diamidino-2-phenylindole (DAPI), respectively. As shown in Figure 4C, it was clearly demonstrated that cells cultured with S-NP at pH 6.8 had much stronger intracellular green fluorescent signals in the cytoplasm when compared with cells treated at other conditions. These results showed that deshielding of the PEG layer at pH 6.8 led to more FAM-siRNA being delivered to the cultured cells by S-NP.

Deshielding the PEG Layer of S-NP Enhances Gene Silencing Efficiency. The efficiency of the tumor acidity-targeted siRNA delivery of S-NP was further evaluated in MDA-MB-231 cells at pH 6.8. Polo-like kinase 1 (Plk1) was selected as the oncogenic target since it is a well-known key regulator of the mitotic progression of mammalian cells and its activity is elevated in many cancer cells.[36] The S-NP or unS-NP was made with siRNA targeting Plk1 (si*Plk1*) and was incubated with MDA-MB-231 cells in complete Dulbecco's modified

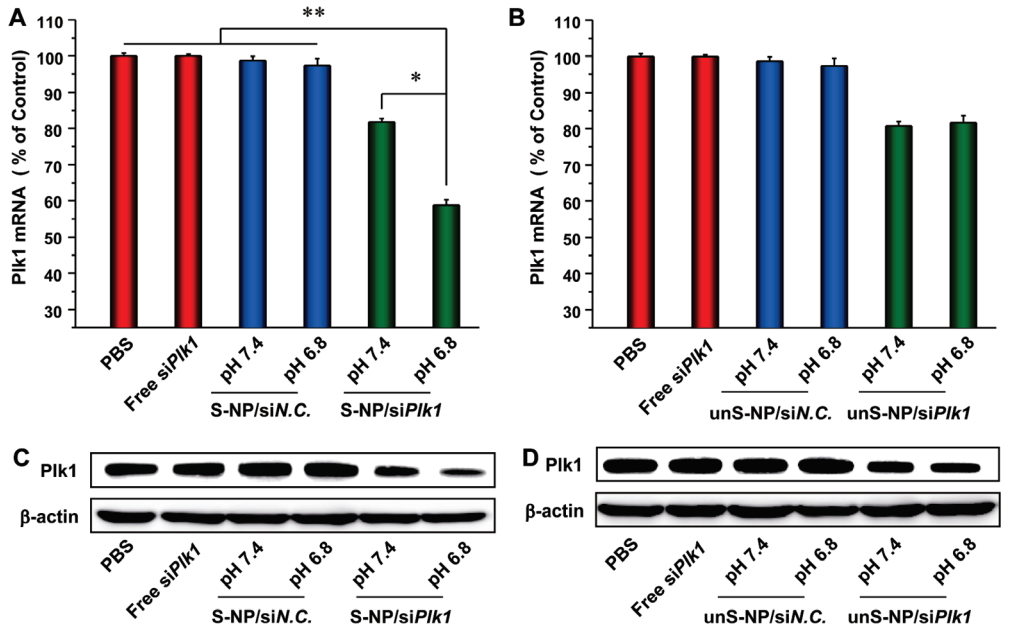

Figure 5. (A,B) Expression levels of Plk1 mRNA in MDA-MB-231 cells after transfection with the S-NP (A) or unS-NP (B). (C,D) Plk1 protein expression in MDA-MB-231 cells after transfection with the S-NP (C) or unS-NP (D). The dose of siRNA was 200 nM when applied. Free si*Plk1* shows that the cells were incubated with si*Plk1*. S-NP/si*Plk1* (or unS-NP/si*Plk1*) and S-NP/si*N.C.* (or unS-NP/si*N.C.*) represent that the cells were transfected with S-NP (or unS-NP) carrying si*Plk1* and si*N.C.*, respectively; pH 7.4 and pH 6.8 represent that the cells were transfected for 2 h in medium at pH 7.4 and pH 6.8, respectively; *$p < 0.01$, **$p < 0.005$ ($n = 3$).

Eagle medium (DMEM) at either pH 7.4 or 6.8 for 2 h. The medium was then replaced with fresh DMEM medium at pH 7.4, and the cells were cultured for a further 22 h. The level of Plk1 mRNA analyzed by quantitative real-time polymerase chain reaction (qRT-PCR) is shown in Figure 5A. The S-NP significantly improved the silencing efficiency of Plk1 expression at pH 6.8 (41.2% down-regulation, $p < 0.01$) compared to that at pH 7.4 (18.3% down-regulation), indicating the benefit of deshielding the PEG layer at pH_e on cell transfection. It is worth noting that S-NP carrying the negative control siRNA (si*N.C.*) did not show a significant gene silencing effect, implying that no nonspecific gene silencing occurred. In contrast, the treatment of MDA-MB-231 cells at pH 6.8 and 7.4 with unS-NP carrying si*Plk1* did not exhibit a significant gene silencing efficiency (19.2% ∝ 18.3% down-regulation) (Figure 5B), which was due to the fact that unS-NP could not re-expose the positively charged surface at either pH.

To examine whether the reduction in Plk1 mRNA was subsequently accompanied by the decreased Plk1 protein expression, the cells were transfected with S-NP or unS-NP at each pH for 2 h, then further incubated with fresh DMEM medium at pH 7.4 for 46 h. The Plk1 protein expression was detected by Western blot analyses. As shown in Figure 5C,D, free si*Plk1* and nanoparticles (both S-NP and unS-NP) carrying si*N.C.* at pH 6.8 and 7.4 did not show any efficiency in the down-regulation of Plk1 protein expression in MDA-MB-231 cells. However, delivery of si*Plk1* by S-NP and unS-NP could knock down Plk1 protein expression to a lower level at each pH. Similarly, S-NP carrying si*Plk1* significantly improved the silencing efficiency of Plk1 protein expression at pH 6.8 compared to the other formulations. The results demonstrated that the detaching of the PEG layer from nanoparticles carrying siRNA could significantly improve target gene silencing efficiency.

Deshielding the PEG Layer of S-NP Promotes Cell Apoptosis. It is well-known that the inhibition of Plk1 expression is associated with the induction of cell apoptosis.[37] Enhancement of Plk1 gene silencing efficiency by S-NP at pH 6.8 led to an elevated induction of cell apoptosis. After 2 h of transfection as described above, MDA-MB-231 cells were further incubated with fresh DMEM medium at pH 7.4 for 46 h, then stained with Annexin-V-FITC and propidine iodide to determine the cell apoptosis. The delivery of si*Plk1* into MDA-MB-231 cells with S-NP at pH 6.8 led to 17.13% cell apoptosis, while only 6.16% cell apoptosis was observed when the cells were treated at pH 7.4 and under other identical conditions (Figure 6). Nevertheless, unS-NP did not induce a remarkably enhanced cell apoptosis at pH 7.4 or 6.8, showing a similar level to S-NP at pH 7.4. Moreover, both S-NP and unS-NP at the same concentration did not show significant cytotoxicity to MDA-MB-231 cells (Figure S3), implying that the enhanced induction of cell apoptosis was not due to the cytotoxicity of the nanoparticles.

Ability of S-NP To Deshield the PEG Layer at Tumor Acidity Enhances Tumor Cell Uptake of siRNA *in Vivo*. In order to evaluate the potential of S-NP for tumor acidity-targeted

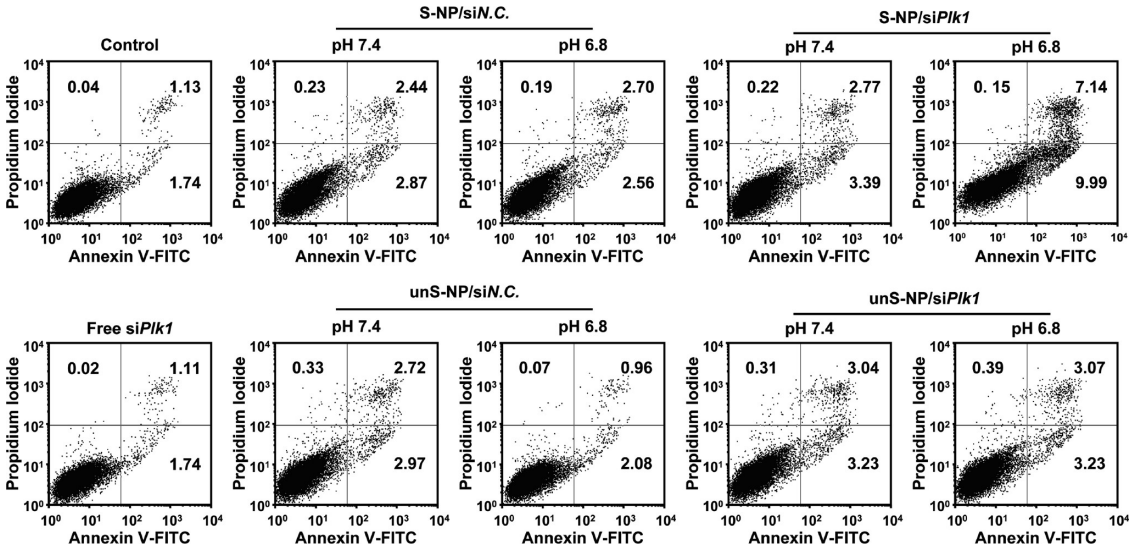

Figure 6. Induction of cell apoptosis following transfection with different formulations at a siRNA dose of 200 nM. Free si*Plk1* shows that the cells were incubated with si*Plk1*. S-NP/si*Plk1* (or unS-NP/si*Plk1*) and S-NP/si*N.C.* (or unS-NP/si*N.C.*) represent that the cells were transfected with S-NP (or unS-NP) carrying si*Plk1* and si*N.C.*, respectively; pH 7.4 and pH 6.8 represent that the cells were transfected for 2 h in medium at pH 7.4 and pH 6.8, respectively. Early apoptotic cells are shown in the lower right quadrant, and late apoptotic cells are shown in the upper right quadrant.

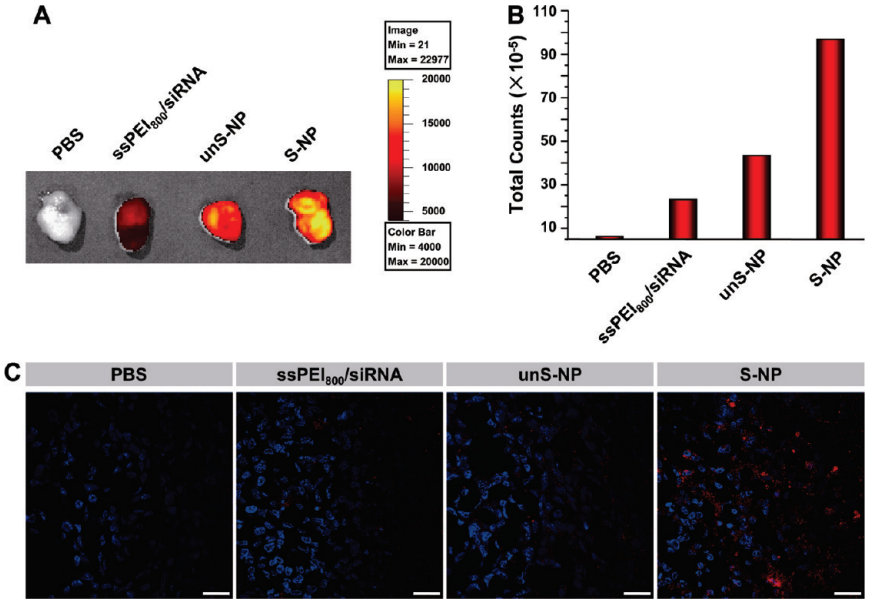

Figure 7. (A) Accumulation of cy5-siRNA in tumor tissue following tail-vein injections of different formulations. The tumor was removed 24 h after the injection, and the fluorescence was recorded. (B) Quantification of cy5-siRNA fluorescence in the tumor tissue as performed in (A) by the total counts. (C) Tumor section observed under confocal microscopy. The cell nuclei were stained with DAPI (blue). The scale bar is 10 μm. ssPEI$_{800}$/siRNA, S-NP, and unS-NP represent where mice were intravenously injected with ssPEI$_{800}$/siRNA, S-NP, and unS-NP carrying cy5-siRNA at a siRNA dose of 3.0 nmol per mouse.

siRNA delivery *in vivo*, we examined the accumulation of siRNA in the tumor 24 h after the intravenous injection of nanoparticles carrying cy5-labeled siRNA (cy5-siRNA) in a mouse bearing an MDA-MB-231 xenograft. As shown in Figure 7A, the strongest fluorescence of cy5-siRNA was detected in the tumor tissue with the intravenous administration of S-NP, whereas the ssPEI$_{800}$/cy5-siRNA nanoparticles showed the weakest fluorescence. With the PEG layer, S-NP and unS-NP markedly minimized nonspecific interactions with serum components during circulation, resulting in a greater accumulation in tumor tissue. Moreover, by deshielding the PEG layer and re-exposing the positively charged surface to the acidic environment of the tumor, S-NP showed stronger fluorescence in the tumor, which should be due to the promoted tumor cellular uptake of siRNA. The quantitative data of fluorescence in the tumor tissue represented by the total counts were analyzed using Living Image 3.1 software, and the results are depicted in Figure 7B.

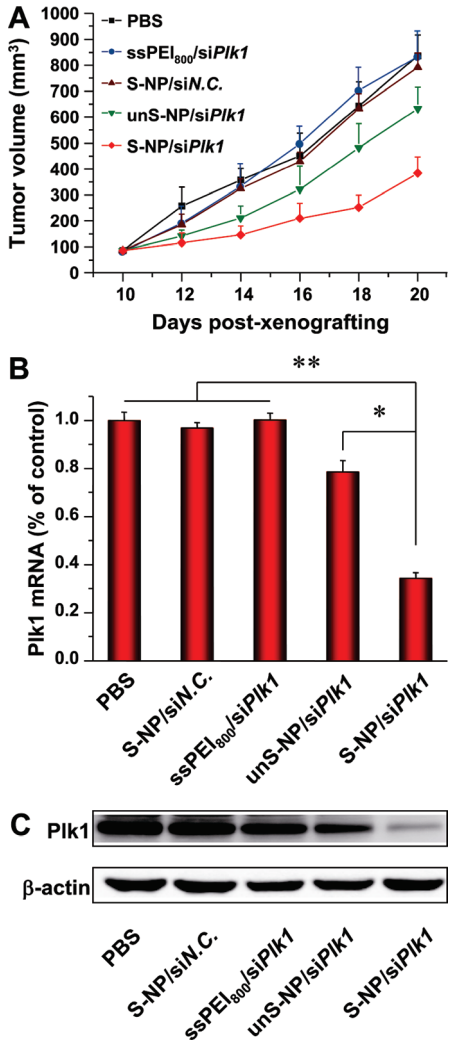

Figure 8. (A) Inhibition of tumor growth in the murine model with the MDA-MB-231 xenograft after treatment with different formulations every other day. (B,C) Expressions of Plk1 mRNA (B) and protein (C) in tumor analyzed 24 h after the last injection. MDA-MB-231 xenograft tumor-bearing mice received one i.v. injection every other day from the 10th day postxenograft implantation in all of the experiments. S-NP/si*Plk1* (or S-NP/si*N.C.*) and unS-NP/si*Plk1* represent where mice were intravenous injected with S-NP carrying si*Plk1* (or si*N.C.*), respectively. The dose of siRNA was 3.0 nmol per mouse per injection; *$p < 0.01$, **$p < 0.005$ ($n = 6$).

The strongest fluorescence of siRNA was detected in the tumor tissue after intravenous injection of S-NP, which was a surprise. We have speculated that the treatment with S-NP or unS-NP should show similar fluorescence in tumors because size and zeta-potential of both nanoparticles were almost the same. However, deshielding the PEG layer from S-NP and re-exposing the positively charged surface by tumor acidity significantly increased tumor cell internalization in animal models, as demonstrated by the confocal microscopic observations of tumor tissue sections (Figure 7C). This observation is correlated well with that by Poon *et al.*[28] Although both S-NP and unS-NP may be equally accumulated within the tumor interstitials *via* the EPR effect, the unS-NPs were less readily internalized but more easily eliminated by the lymphatic system. On the contrary, S-NPs can deshield the PEG layer, and the cell internalization was promoted due to the exposure of positively charged surface, which decreased the elimination and led to strongest fluorescence in the tumor site.

S-NPs Carrying si*Plk1* Significantly Promote Antitumor Effect Following Intravenous Injection. The advantages of S-NP in tumor acidity-targeted siRNA delivery will potentially enhance the efficiency of interfering RNA in cancer therapy *in vivo*. To demonstrate this, we examined the antitumor growth effect in mice with MDA-MB-231 xenografts by tail-vein injections of different formulations carrying si*Plk1*. As illustrated in Figure 8A, treatment with the ssPEI$_{800}$/si*Plk1* nanoparticles did not show tumor growth inhibition in comparison to PBS. Delivery of si*Plk1* with unS-NP only slightly inhibited tumor growth in the murine model. However, delivery of si*Plk1* with S-NP to tumor-bearing mice showed a significant inhibition of tumor growth. It should be noted that the injection of S-NP carrying si*N.C.* did not inhibit tumor growth, indicating that the antitumor effect was siRNA sequence-specific.

To further evaluate whether retarded tumor growth by S-NPs carrying si*Plk1* was related to Plk1 gene silencing in tumor cells, the tumor mass was excised 24 h after the last injection. Plk1 expression at mRNA and protein levels in the tumors was analyzed by qRT-PCR and Western blot analyses. Mice treated by S-NP carrying si*Plk1* showed reduced Plk1 mRNA levels (~33% of the PBS control, $p < 0.005$, Figure 8B), whereas that of the unS-NP/si*Plk1* at the same siRNA dose exhibited only slight down-regulated Plk1 (about 79% of the PBS control). Besides, the other controls did not cause this effect. Analysis of Plk1 protein of each tumor mass by Western blot analyses showed consistent knockdown efficiency. As shown in Figure 8C, the tumor of mice treated with unS-NP/si*Plk1* at the same siRNA dose exhibited only slight down-regulation of Plk1 protein expression. However, significant down-regulation of Plk1 protein expression occurred when the S-NP carrying si*Plk1* was used. In contrast, Plk1 protein levels remained unchanged in the tumor of mice treated with free si*Plk1* and S-NP carrying si*N.C.* The results demonstrated that significant inhibition of tumor growth was achieved by treatment with S-NP carrying si*Plk1* due to Plk1 gene silencing in tumor cells.

Cell proliferation in the tumor tissue after treatment was analyzed by immunohistochemical staining of the proliferating cell nuclear antigen (PCNA). As shown in Figure 9, a decrease in PCNA-positive tumoral cells (brown) in tumor tissue is shown upon treatment with unS-NP carrying si*Plk1* when compared with PBS treatment. Moreover, S-NP carrying si*Plk1* treatment was more effective in preventing tumor cell proliferation

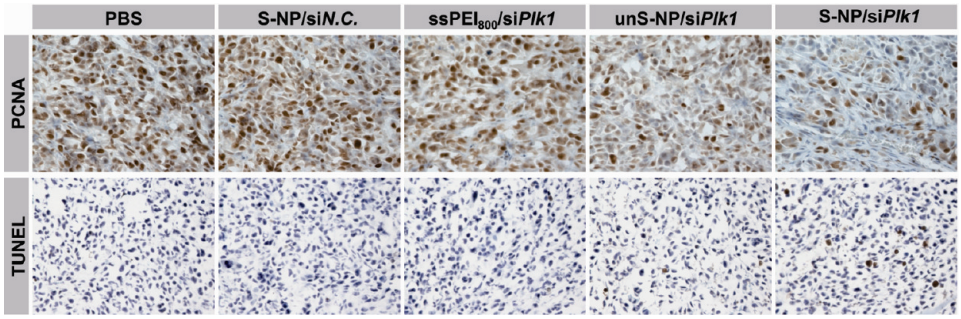

Figure 9. PCNA and TUNEL analyses of tumor tissues after treatments with various formulations. The tumor tissues were collected 24 h after the last injection. S-NP/si*Plk1* (or S-NP/si*N.C.*) and unS-NP/si*Plk1* represent where mice were intravenously injected with S-NP carrying si*Plk1* (or si*N.C.*), respectively.

with an exhibition of less PCNA-positive tumoral cells compared with unS-NP carrying si*Plk1* treatment. Cell apoptosis in the tumor tissue after treatments was detected using the terminal deoxynucleotidyl transferase-mediated dUTP nick end-labeling (TUNEL) assay. Corresponding with the tumor growth inhibition, treatment with S-NP carrying si*Plk1* increased TUNEL-positive tumoral cells (brown). It is worth noting that ssPEI$_{800}$/si*Plk1* and S-NP carrying si*N.C.* did not significantly affect the percentages of the proliferating PCNA-positive tumoral cells and TUNEL-positive tumoral cells.

In summary, we developed sheddable ternary nanoparticles for tumor acidity-targeted siRNA delivery and showed that the shell shedding of nanoparticles promotes gene silencing efficiency and tumor growth inhibition. The nanoparticles can respond to the extracellular pH of tumor tissue but not to the pH of normal blood. With a specific response to tumor acidity, the nanoparticles showed enhanced uptake by tumor cells, promoting the efficiency of siRNA in cancer therapy. We demonstrate proof of principle that the efficiency of cationic polymers with siRNAs in cancer therapy can be significantly improved by coating their surfaces with a tumor acidity-activated sheddable PEG layer. This idea could be extended to nanoparticle delivery systems for a broad range of drugs. In addition, a more comprehensive study of such nanoparticle systems is planned for future work to gain a better understanding of the efficacy of such systems in overcoming the barriers of systemic drug delivery to tumors, including the extended blood circulation, accumulation in tumor tissue, internalization by tumoral cells, and intracellular drug release.

MATERIALS AND METHODS

Materials and Characterization. Dulbecco's modified Eagle's medium (DMEM, Gibco, Grand Island) and L-glutamine were purchased from Gibco BRL (Germany). The Lipofectamine 2000 transfection kit and DAPI from Invitrogen (Carlsbad, USA) were used as suggested by the supplier. Fluorescently labeled FAM-siRNA and cy5-siRNA, negative control siRNA (si*N.C.*, antisense strand, 5′-ACGUGACACGUUCGGAGAAdTdT-3′), and siRNA targeting Plk1 mRNA (si*Plk1*, antisense strand, 5′-UAAGGAGGGUGAUCUUCUUCAdTdT-3′) were synthesized by Suzhou Ribo Life Science Co. (Kunshan, China).

Zeta-potentials and particle size measurements were conducted by using a zeta-potential analyzer with dynamic light scattering (DLS) capability, with a Malvern Zetasizer Nano ZS90, a He−Ne laser (633 nm), and 90° collecting optics. The average values from the intensity statistics of a total of 20 runs of 30 s each were used. Data were analyzed using Malvern Dispersion Technology Software 4.20 and expressed as the average diameter ± the width of the distribution.

Preparation of S-NP. The S-NP was prepared by adding PPC-DA solution to positively charged ssPEI$_{800}$/siRNA nanoparticles. The PPC-DA (0.1 mL, 5 mg/mL in water) was added to an aqueous solution of ssPEI$_{800}$/siRNA (N/P = 16/1) nanoparticles in 0.1 mL of RNase free water. The final concentration of siRNA in the solution was 5 μM. This PPC-DA/ssPEI$_{800}$/siRNA nanoparticles at C/N/P = 32/16/1 were further denoted as S-NP. Here, C/N/P was defined as the molar ratio of carboxyl in the PPC-DA or PPC-SA, amine in the ssPEI$_{800}$, and phosphate in the siRNA. The S-NP was used after 15 min incubation at room temperature.

Preparation of unS-NP. The unS-NP was prepared by a similar procedure to the S-NP, by replacing the PPC-DA with PPC-SA. The final C/N/P ratio was 32/16/1. The average size and zeta-potential of unS-NP were 93.2 ± 18.6 (PDI = 0.217) nm and −14.0 mV, respectively, similar to that of S-NP.

Characterization of the Stability of Nanoparticles. The ssPEI$_{800}$/siRNA nanoparticles (N/P = 16/1), unS-NP, or S-NP were gently mixed with BSA (Sigma-Aldrich) solution in phosphate buffered saline (PBS, pH 7.4, 0.01 M). The final concentrations of siRNA and BSA were 0.04 and 0.25 mg mL^{-1}, respectively. The mean diameters of nanoparticles after different periods of incubation were monitored by a Malvern Zetasizer Nano ZS90 apparatus as described above. Transmission electronic microscopy was performed on a JEOL-2010 microscope with an accelerating voltage of 200 kV.

Zeta-Potential Measurements of S-NP and unS-NP at Different pH. The unS-NP or S-NP was incubated in PBS (0.01 M) at pH 6.8 or 7.4 at 37 °C. The final concentration of siRNA was 1.0 μM in the solution. At designated time intervals, aliquot of the nanoparticle solution was withdrawn and the zeta-potential was measured with a Malvern Zetasizer Nano ZS90. Each measurement was performed for 30 runs.

Cell Culture. The human breast cancer cell line MDA-MB-231 from the American Type Culture Collection (ATCC) was used to evaluate the potency of the delivery system both *in vitro* and *in vivo*. Cells were cultured in DMEM (Gibco, Carlsbad, CA) with 10% fetal bovine serum (Gibco) at 37 °C with 5% CO_2 humidified atmosphere.

Analyses of Cellular Uptake after Treatment with S-NP or unS-NP at Different pH. For flow cytometric analysis, MDA-MB-231 cells

were seeded into 24-well plates at 1×10^5 cells per well in 0.5 mL complete DMEM medium and cultured at 37 °C in 5% CO_2 humidified atmosphere for 24 h. The medium was replaced with complete DMEM medium (pH 7.4 or 6.8) containing S-NP or unS-NP. The final concentration of FAM-siRNA in the culture medium was 200 nM in all of the experiments. The cells were incubated at 37 °C for 2 h at either pH 7.4 or 6.8, then the cells were rinsed twice with cold PBS (pH 7.4). The cells were trypsinized, washed with cold PBS (pH 7.4), filtered through 35 μm nylon mesh, and subjected to flow cytometric analysis using a BD FACSCalibur flow cytometer (BD Bioscience, Bedford, MA). The results were analyzed using WinMDI 2.9 software.

For microscopic observation, MDA-MB-231 cells (1×10^5 cells/well) were seeded on coverslips in a 24-well plate and incubated for 24 h. The medium was replaced with complete DMEM medium (pH 7.4 or 6.8) containing S-NP or unS-NP. The final concentration of FAM-siRNA in the culture medium was 200 nM in all of the experiments. The cells were incubated at 37 °C for 2 h at either pH 7.4 or 6.8, then washed twice with PBS, and fixed with 4% formaldehyde for 15 min at room temperature. The cells were stained with Alexa Fluor 568 phalloidin (Invitrogen, Carlsbad, USA) for the cytoskeleton and counterstained with DAPI for cell nuclei according to the standard protocol provided by the suppliers. Coverslips were mounted on glass microscope slides with a drop of antifade mounting media (Sigma-Aldrich) to reduce fluorescence photobleaching. The cellular uptake of nanoparticles was visualized by a confocal laser scanning microscope (LSM 710, Carl Zeiss Inc., Jena, Germany).

***In Vitro* Transfection and Analysis of Gene Expression.** MDA-MB-231 cells were seeded into 6-well plates at 4×10^5 cells per well in 2.0 mL of complete DMEM medium and cultured at 37 °C in 5% CO_2 humidified atmosphere 24 h. The medium was replaced with complete DMEM medium (pH 7.4 or 6.8) containing S-NP or unS-NP. The si*Plk1* or si*N.C.* was used in the experiment, and the final concentration of siRNA in the culture medium was 200 nM in all of the experiments. The cells were incubated at 37 °C for 2 h at either pH 7.4 or 6.8, then the culture medium was replaced with fresh complete DMEM medium at pH 7.4. After further incubation for 22 h (for mRNA isolation) or 46 h (for protein extraction) at 37 °C, the cellular levels of Plk1 mRNA and protein were assessed using qRT-PCR and Western blot, respectively.

In qRT-PCR analysis, the cells were collected and total RNA from transfected cells was isolated using an RNeasy mini-kit (Qiagen, Valencia, CA) according to the protocol of the manufacturer. Two micrograms of total RNA was transcribed into cDNA using the PrimeScript 1st Strand cDNA Synthesis Kit (Takara, Dalian, China). Thereafter, 2 μL of cDNA was subjected to quantitative real-time PCR analysis targeting Plk1 and glyceraldehyde 3-phosphate dehydrogenase (GAPDH) using the SYBR Premix Ex Taq (Perfect Real Time) (Takara, Dalian, China). Analysis was performed using the Applied Biosystems StepOne Real-Time PCR Systems. Relative gene expression values were determined by the $\Delta\Delta$CT method using StepOne Software v2.1 (Applied Biosystems). Data are presented as the fold difference in Plk1 expression normalized to the housekeeping gene GAPDH as the endogenous reference and relative to the untreated control cells. The primers used in the quantitative real-time PCR for Plk1 and GAPDH were 5′-AGCCTGAGGCCCGATACTACCTAC-3′ (Plk1-forward), 5′-ATTAGGAGTCCCACACAGGGTCTTC-3′ (Plk1-reverse), and 5′-TTCACCACCATGGAGAAGGC-3′ (GAPDH-forward), 5′-GGCATGGACTGTGGTCATGA-3′ (GAPDH-reverse). PCR parameters consisted of 30 s of *Taq* activation at 95 °C, followed by 40 cycles of PCR at 95 °C × 5 s, 60 °C × 30 s, and 1 cycle of 95 °C × 15 s, 60 °C × 60 s, and 95 °C × 15 s. Standard curves were generated, and the relative amount of target gene mRNA was normalized to GAPDH mRNA. Specificity was verified by melt curve analysis.

In Western blot analysis, transfected cells were first washed twice with cold PBS and then resuspended in 50 μL of lysis buffer (50 mM HEPES, pH 7.5, 150 mM NaCl, 1% Triton X-100, 10% glycerol, 1.5 mM $MgCl_2$, 1 mM EGTA) freshly supplemented with Roche's Complete Protease Inhibitor Cocktail Tablets. The cell lysates were incubated on ice for 1 h and vortexed every 5 min. The lysates were then clarified by centrifugation for 10 min at 12 000*g*. The protein concentration was determined using the BCA protein assay kit (lot 23250, Thermo, USA). Total protein (100 μg) was separated on 12% bis-Tris-polyacrylamide gels and then transferred (at 300 mA for 45 min) to Immobilon-P membranes (Millipore, Bedford, MA). After incubation in 5% BSA in phosphate buffered saline with Tween-20 (PBST, pH 7.2) for 2 h, the membranes were incubated in 1% BSA in PBS with monoclonal antibodies against Plk1 (1:1000) overnight. After incubation in 1% BSA with goat anti-mouse IgG-HRP antibody (1:10000) for 30 min, bands were visualized using ImageQuant LAS 4000 mini (GE Healthcare).

Cell Apoptosis Assay. MDA-MB-231 cells were seeded into 6-well plates at 2×10^5 cells per well in 2.0 mL of complete DMEM medium and cultured at 37 °C in 5% CO_2 humidified atmosphere for 24 h. The medium was replaced with complete DMEM medium (pH 7.4 or 6.8) containing S-NP or unS-NP. The si*Plk1* or si*N.C.* was used in the experiment, and the final concentration of siRNA in the culture medium was 200 nM in all of the experiments. The cells were incubated at 37 °C for 2 h at either pH 7.4 or 6.8, then the culture medium was replaced with fresh complete DMEM medium at pH 7.4. After further incubation for 46 h at 37 °C, the cells were collected and the apoptotic cells were detected by flow cytometry after treatment with the Annexin V-FITC apoptosis detection kit I (BD Biosciences) according to the suggested procedure. The results were analyzed using WinMDI 2.9 software.

Tumoral Cellalur Uptake of Nanoparticles *in Vivo*. BALB/c nude mice (6 weeks old) were purchased from the Shanghai Experimental Animal Centre of the Chinese Academy of Sciences (Shanghai, China), and all animals received care in compliance with the guidelines outlined in the Guide for the Care and Use of Laboratory Animals. The procedures were approved by the University of Science and Technology of China Animal Care and Use Committee.

The xenograft tumor model was generated by subcutaneous injection of MDA-MB-231 cells (5×10^6 for each mouse) in the mammary fat pad of the mouse. When the tumor volume was about 100 mm^3, the mice were intravenous injected with 200 μL of $ssPEI_{800}$/cy5-siRNA nanoparticles, S-NP, or unS-NP, containing 40 μg of cy5-siRNA (3.0 nmol) or PBS (pH 7.4). After 24 h, the mice were sacrificed and the solid tumor tissues were harvested. Image acquisition was performed on a Xenogen IVIS Lumina system (Caliper Life Sciences, USA). Results were analyzed using Living Image 3.1 software (Caliper Life Sciences).

To determine cy5-siRNA distribution in tumor tissue, the tumor was fixed by 4% paraformaldehyde at 4 °C for 2 h and then treated with 30% sucrose at 4 °C overnight. The tumor tissues were frozenly sectioned into 5 μm slices and air-dried for 61 h. Then, the slices were stained with DAPI. Finally, the slices were mounted and observed by Zeiss LSM-710 confocal laser scanning microscope.

Tumor Suppression Study. The murine tumor model with MDA-MB-231 xenograft was established as described above. When the tumor volume was around 100 mm^3 at 10 days after cell implantation, the mice were randomly divided into five groups (six mice per group) and treated with PBS, $ssPEI_{800}$/si*Plk1* nanoparticles, unS-NP or S-NP carrying si*Plk1* or control si*N.C.* by intravenous injection. The mouse received injection once every other day. The dose of siRNA of each injection was 40 μg per mouse (3.0 nmol). Tumor growth was monitored by measuring the perpendicular diameter of the tumor using calipers. The estimated volume was calculated according to the formula: tumor volume (mm^3) = 0.5 × length × $width^2$.

Detection of Plk1 Expression in Tumor Tissues. For Plk1 mRNA analysis, tumor tissues were collected 24 h after the last treatment, lysed using an RNeasy mini-kit. The mRNA was collected and analyzed by qRT-PCR as describe above.

To determine Plk1 protein expression in tumor tissue after treatments, tumor tissues were collected and lysed in 100 μL tissue lysis buffer (50 mM HEPES, pH 7.5, 150 mM NaCl, 1 mM EGTA, 2.5 mM EDTA, 10% glycerol, 0.1% Tween 20, 1 mM dithiothreitol, 10 mM glycerol 2-phosphate, 1 mM NaF, and 0.1 mM Na_3VO_4) freshly supplemented with Roche's Complete Protease Inhibitor Cocktail Tablets. The lysates were incubated on ice for a total of 30 min and vortexed every 5 min. The lysates

were centrifuged for 10 min at 12 000*g*. Then the protein was detected by Western blot analyses as describe above.

Immunohistochemical Analysis. Twenty four hours after the last treatment, animals were sacrificed and tumor tissues were excised. The tissues were fixed in 4% formaldehyde and embedded in paraffin for analysis. The paraffin-embedded 5 μm tumor sections were obtained for immunohistochemical analysis.

To analyze the PCNA, deparaffinized slides were boiled for 5 min in 0.01 M sodium citrate buffer (pH 6.0), in a pressure cooker for antigen retrieval. Subsequently, slides were allowed to cool for another 5 min in the same buffer. After several rinses in PBS and pretreatment with blocking medium for 5 min, slides were incubated with PCNA antibody (Maxim Biotech., Fuzhou, China) diluted at 1:300 in antibody diluent solution for 20 min at room temperature and then at 4 °C overnight. After washing slides in Tris-buffered saline, a streptavidin−biotin system was used according to the manufacturer's instructions (BioGenex, San Ramon, USA). The slides were counterstained using Aquatex (Merck, Gernsheim, Germany).

The apoptosis of tumor cells following treatments was determined using TUNEL method according to the manufacturer's instructions (Roche, Basel, Switzerland). All sections were examined under a Nikon TE2000 microscope (Tokyo Prefecture, Japan).

Statistical Analysis. The statistical significance of treatment was assessed using the Student's *t* test; $p < 0.05$ was considered statistically significant in all analyses (95% confidence level).

Acknowledgment. This work was supported by the National Basic Research Program of China (973 Programs, 2010CB934001 and 2012CB932502), the National Natural Science Foundation of China (51125012, 50733003), the Fundamental Research Funds for the Central Universities (WK2070000008), and Open Project of State Key Laboratory of Supramolecular Structure and Materials (SKLSSM201117).

Supporting Information Available: Syntheses procedures and characterization of procedure polymers, additional experimental methods, and figures. This material is available free of charge *via* the Internet at http://pubs.acs.org.

REFERENCES AND NOTES

1. Song, E. W.; Lee, S. K.; Wang, J.; Ince, N.; Ouyang, N.; Min, J.; Chen, J. S.; Shankar, P.; Lieberman, J. RNA Interference Targeting Fas Protects Mice from Fulminant Hepatitis. *Nat. Med.* **2003**, *9*, 347–351.
2. Woodrow, K. A.; Cu, Y.; Booth, C. J.; Saucier-Sawyer, J. K.; Wood, M. J.; Saltzman, W. M. Intravaginal Gene Silencing Using Biodegradable Polymer Nanoparticles Densely Loaded with Small-Interfering RNA. *Nat. Mater.* **2009**, *8*, 526–533.
3. Davis, M. E.; Zuckerman, J. E.; Choi, C. H. J.; Seligson, D.; Tolcher, A.; Alabi, C. A.; Yen, Y.; Heidel, J. D.; Ribas, A. Evidence of RNAi in Humans from Systemically Administered siRNA *via* Targeted Nanoparticles. *Nature* **2010**, *464*, 1067–1070.
4. Kumar, P.; Ban, H. S.; Kim, S. S.; Wu, H. Q.; Pearson, T.; Greiner, D. L.; Laouar, A.; Yao, J. H.; Haridas, V.; Habiro, K.; *et al.* T Cell-Specific siRNA Delivery Suppresses HIV-1 Infection in Humanized Mice. *Cell* **2008**, *134*, 577–586.
5. Bumcrot, D.; Manoharan, M.; Koteliansky, V.; Sah, D. W. Y. RNAi Therapeutics: A Potential New Class of Pharmaceutical Drugs. *Nat. Chem. Biol.* **2006**, *2*, 711–719.
6. Pecot, C. V.; Calin, G. A.; Coleman, R. L.; Lopez-Berestein, G.; Sood, A. K. RNA Interference in the Clinic: Challenges and Future Directions. *Nat. Rev. Cancer* **2011**, *11*, 59–67.
7. Zintchenko, A.; Philipp, A.; Dehshahri, A.; Wagner, E. Simple Modifications of Branched PEI Lead to Highly Efficient siRNA Carriers with Low Toxicity. *Bioconjugate Chem.* **2008**, *19*, 1448–1455.
8. Werth, S.; Urban-Klein, B.; Dai, L.; Hobel, S.; Grzelinski, M.; Bakowsky, U.; Czubayko, F.; Aigner, A. A Low Molecular Weight Fraction of Polyethylenimine (PEI) Displays Increased Transfection Efficiency of DNA and siRNA in Fresh or Lyophilized Complexes. *J. Controlled Release* **2006**, *112*, 257–270.
9. Kim, H. J.; Ishii, A.; Miyata, K.; Lee, Y.; Wu, S.; Oba, M.; Nishiyama, N.; Kataoka, K. Introduction of Stearoyl Moieties into a Biocompatible Cationic Polyaspartamide Derivative, PAsp(DET), with Endosomal Escaping Function for Enhanced siRNA-Mediated Gene Knockdown. *J. Controlled Release* **2010**, *145*, 141–148.
10. Nomoto, T.; Matsumoto, Y.; Miyata, K.; Oba, M.; Fukushima, S.; Nishiyama, N.; Yamasoba, T.; Kataoka, K. *In Situ* Quantitative Monitoring of Polyplexes and Polyplex Micelles in the Blood Circulation using Intravital Real-Time Confocal Laser Scanning Microscopy. *J. Controlled Release* **2011**, *151*, 104–109.
11. Ko, Y. T.; Bhattacharya, R.; Bickel, U. Liposome Encapsulated Polyethylenimine/ODN Polyplexes for Brain Targeting. *J. Controlled Release* **2009**, *133*, 230–237.
12. Jeong, J. H.; Kim, S. W.; Park, T. G. Molecular Design of Functional Polymers for Gene Therapy. *Prog. Polym. Sci.* **2007**, *32*, 1239–1274.
13. Davis, M. E.; Chen, Z.; Shin, D. M. Nanoparticle Therapeutics: An Emerging Treatment Modality for Cancer. *Nat. Rev. Drug Discovery* **2008**, *7*, 771–782.
14. Gao, K.; Huang, L. Nonviral Methods for siRNA Delivery. *Mol. Pharmaceutics* **2009**, *6*, 651–658.
15. Ogris, M.; Brunner, S.; Schuller, S.; Kircheis, R.; Wagner, E. PEGylated DNA/Transferrin-PEI Complexes: Reduced Interaction with Blood Components, Extended Circulation in Blood and Potential for Systemic Gene Delivery. *Gene Ther.* **1999**, *6*, 595–605.
16. Hatakeyama, H.; Akita, H.; Harashima, H. A Multifunctional Envelope Type Nano Device (MEND) for Gene Delivery to Tumors Based on the EPR Effect: A Strategy for Overcoming the PEG Dilemma. *Adv. Drug Delivery Rev.* **2011**, *63*, 152–160.
17. Mishra, S.; Webster, P.; Davis, M. E. PEGylation Significantly Affects Cellular Uptake and Intracellular Trafficking of Non-viral Gene Delivery Particles. *Eur. J. Cell Biol.* **2004**, *83*, 97–111.
18. Gratton, S. E. A.; Ropp, P. A.; Pohlhaus, P. D.; Luft, J. C.; Madden, V. J.; Napier, M. E.; DeSimone, J. M. The Effect of Particle Design on Cellular Internalization Pathways. *Proc. Natl. Acad. Sci. U.S.A.* **2008**, *105*, 11613–11618.
19. Edinger, D.; Wagner, E. Bioresponsive Polymers for the Delivery of Therapeutic Nucleic Acids. *WIREs Nanomed. Nanobiotechnol.* **2011**, *3*, 33–46.
20. Romberg, B.; Hennink, W. E.; Storm, G. Sheddable Coatings for Long-Circulating Nanoparticles. *Pharm. Res.* **2008**, *25*, 55–71.
21. Yamagata, M.; Hasuda, K.; Stamato, T.; Tannock, I. F. The Contribution of Lactic Acid to Acidification of Tumours: Studies of Variant Cells Lacking Lactate Dehydrogenase. *Br. J. Cancer* **1998**, *77*, 1726–1731.
22. Helmlinger, G.; Schell, A.; Dellian, M.; Forbes, N. S.; Jain, R. K. Acid Production in Glycolysis-Impaired Tumors Provides New Insights into Tumor Metabolism. *Clin. Cancer Res.* **2002**, *8*, 1284–1291.
23. Vander, H. M. G.; Cantley, L. C.; Thompson, C. B. Understanding the Warburg Effect: The Metabolic Requirements of Cell Proliferation. *Science* **2009**, *324*, 1029–33.
24. Lee, E. S.; Shin, H. J.; Na, K.; Bae, Y. H. Poly(L-histidine)-PEG Block Copolymer Micelles and pH-Induced Destabilization. *J. Controlled Release* **2003**, *90*, 363–374.
25. Min, K. H.; Kim, J. H.; Bae, S. M.; Shin, H.; Kim, M. S.; Park, S.; Lee, H.; Park, R. W.; Kim, I. S.; Kim, K.; *et al.* Tumoral Acidic pH-Responsive MPEG-poly(β-amino ester) Polymeric Micelles for Cancer Targeting Therapy. *J. Controlled Release* **2010**, *144*, 259–266.
26. Lee, E. S.; Na, K.; Bae, Y. H. Super pH-Sensitive Multifunctional Polymeric Micelle. *Nano Lett.* **2005**, *5*, 325–329.
27. Sethuraman, V. A.; Bae, Y. H. TAT Peptide-Based Micelle System for Potential Active Targeting of Anti-Cancer Agents to Acidic Solid Tumors. *J. Controlled Release* **2007**, *118*, 216–224.
28. Poon, Z.; Chang, D.; Zhao, X. Y.; Hammond, P. T. Layer-by-Layer Nanoparticles with a pH-Sheddable Layer for *In Vivo* Targeting of Tumor Hypoxia. *ACS Nano* **2011**, *5*, 4284–4292.

29. Sethuraman, V. A.; Na, K.; Bae, Y. H. pH-Responsive Sulfonamide/PEI System for Tumor Specific Gene Delivery: An *In Vitro* Study. *Biomacromolecules* **2006**, *7*, 64–70.
30. Du, J. Z.; Du, X. J.; Mao, C. Q.; Wang, J. Tailor-Made Dual pH-Sensitive Polymer-Doxorubicin Nanoparticles for Efficient Anticancer Drug Delivery. *J. Am. Chem. Soc.* **2011**, *133*, 17560–17563.
31. Breunig, M.; Hozsa, C.; Lungwitz, U.; Watanabe, K.; Umeda, I.; Kato, H.; Goepferich, A. Mechanistic Investigation of Poly(ethylene imine)-Based siRNA Delivery: Disulfide Bonds Boost Intracellular Release of the Cargo. *J. Controlled Release* **2008**, *130*, 57–63.
32. Choi, K. Y.; Min, K. H.; Yoon, H. Y.; Kim, K.; Park, J. H.; Kwon, I. C.; Choi, K.; Jeong, S. Y. PEGylation of Hyaluronic Acid Nanoparticles Improves Tumor Targetability *in Vivo*. *Biomaterials* **2011**, *32*, 1880–1889.
33. Meyer, M.; Philipp, A.; Oskuee, R.; Schmidt, C.; Wagner, E. Breathing Life into Polycations: Functionalization with pH-Responsive Endosomolytic Peptides and Polyethylene Glycol Enables siRNA Delivery. *J. Am. Chem. Soc.* **2008**, *130*, 3272–3273.
34. Du, J. Z.; Sun, T. M.; Song, W. J.; Wu, J.; Wang, J. A Tumor-Acidity-Activated Charge-Conversional Nanogel as an Intelligent Vehicle for Promoted Tumoral-Cell Uptake and Drug Delivery. *Angew. Chem., Int. Ed.* **2010**, *49*, 3621–3626.
35. Cho, E. C.; Xie, J. W.; Wurm, P. A.; Xia, Y. N. Understanding the Role of Surface Charges in Cellular Adsorption *versus* Internalization by Selectively Removing Gold Nanoparticles on the Cell Surface with a I_2/KI Etchant. *Nano Lett.* **2009**, *9*, 1080–1084.
36. Liu, X. Q.; Erikson, R. L. Polo-like Kinase (Plk) 1 Depletion Induces Apoptosis in Cancer Cells. *Proc. Natl. Acad. Sci. U.S.A.* **2003**, *100*, 5789–5794.
37. Judge, A. D.; Robbins, M.; Tavakoli, I.; Levi, J.; Hu, L.; Fronda, A.; Ambegia, E.; McClintock, K.; MacLachlan, I. Confirming the RNAi-Mediated Mechanism of Action of siRNA-Based Cancer Therapeutics in Mice. *J. Clin. Invest.* **2009**, *119*, 661–673.